Study on the Effect of Sidebands of KSTAR-like Traveling Wave Antenna Power Spectrum on Helicon Wave Current Drive in EXL-50U Spherical Torus Plasma*

Dan Du,[1] Cui Yu,[2] Sheng Deng,[3, †] Qing-Xi Yang,[3] Gao-Kui He,[4] J.G. Kwak,[5] H.H. Wi,[5] Jing-Chun Li,[6] Xin Zhao,[7] Zi-Wen Huang,[8] and Wen-Jun Yang[2]

[1]*Department of Mathematics and Physics, University of South China, Hengyang 421001, China*
[2]*Department of Electrical Engineering, University of South China, Hengyang 421001, China*
[3]*Institute of Plasma Physics, Hefei Institutes of Physical Science, Chinese Academy of Sciences, Hefei 230031, China*
[4]*Institute of Comprehensive Nuclear Technology, China Institute of Atomic Energy, Beijing 102413, China*
[5]*Korea Institute of Fusion Energy, Daejeon 34133, Republic Of Korea*
[6]*Department of Earth and Space Sciences, Southern University of Science and Technology, Shenzhen 518055, China*
[7]*ENN Science and Technology Development Co. Ltd., Langfang 065001, China*
[8]*Department of Nuclear Science and Technology, University of South China, Hengyang 421001, China*

This paper investigates the influence of sidebands of two KSTAR-like traveling wave antennas (TWAs) spectra on helicon current drive (HCD) in spherical tokamak EXL-50U. First, two sets of 476 MHz KSTAR-like TWAs are designed based on optimized parameters obtained through extensive scanning, whose spectra have the same parallel refractive index $N_{\|} = -3.2$ corresponding to the main peak and different sidebands. Then, comparing the current driven by them with Gaussian-like spectrum, the effects of sidebands of these two TWAs spectra on HCD are discussed. The analysis reveals that under medium-density low magnetic field and low-density high magnetic field conditions, the sidebands have a significant impact on HCD, with a maximum driven current absolute difference of 178 kA for two KSTAR-like TWAs spectra and Gaussian-like spectrum with the same injection power. Higher temperature leads to an increase in the impact of sidebands on HCD. The sidebands not only affect the magnitude of HCD, but also cause the current peak to shift towards the plasma center or edge. Under certain conditions, narrow sidebands with parallel refractive index close to the strong Landau damping condition may be beneficial to improve the driven current magnitude and local control. Relevant research provides certain guidance for the design of RF antenna and HCD experiments.

Keywords: Helicon current drive, Traveling wave antenna, Sidebands, Localization of current distribution

I. INTRODUCTION

The non-inductive current drive in plasma is one of the important issues for achieving stable operation of fusion devices based on tokamak [1–4]. To maintain a reverse shear or negative shear magnetic field configuration for high performance and steady-state operation, the current should be off-axis. There are various methods to make the current drive utilizing auxiliary heating in tokamak plasmas, and helicon current drive (HCD), also known as fast wave current drive (CD) in the lower hybrid range of frequencies, is regarded as a promising tool for driving off-axis currents in reactor-grade plasma.

In high beta plasma, due to the large harmonic number (the angular frequency ω is about 30-50 times the ion cyclotron frequency ω_{ci} [3, 5], helicon wave's ion cyclotron damping can be quite weak. In constrast, its electron damping can be strong. Since the damping of helicon wave on electrons is so strong at high beta, the wave power can be significantly damped before it reaches the center of the plasma, which allows for the possibilities of off-axis current drive and radial deposition control via control of the launched wave spectrum [5].

Some progress has been made in the field of helicon wave heating and current drive. The importance of helicon wave for current drive was first realized through ARIES reactor studies [6]. HCD experiments in NSTX spherical tokamak demonstr- ated the central electron temperatures of 4 keV had been achieved, and the value of driven current was about 100 kA [5]. Traveling wave antennas (TWA) have many advantages, such as load resilience, narrow $N_{\|}$ spectrum, good plasma coupling and excellent impedance matching capability [7, 8]. A 12-element combline TWA exhibited the expected characteristics, and obtained at least 10 keV high energy electrons in the plasma core during JFT-2M helicon current drive experiments. Experiments with the low power (100-300 kW) combline-type TWA and strong coupling have confirmed the feasibility of the helicon current drive system of KSTAR [9] and DIII-D [10]. Recently, a newly MW-level helical type TWA and 30-module TWA for helicon wave current drive have been successfully installed in KSTAR and DIII-D respectively [8, 9, 11].

A series of numerical calculations have verified that the high efficiency of helicon wave heating and current drive in tokamaks by the ray-tracing code GENRAY using the Ehst-Karney formula, the Fokker-Planck code CQL3D containing the quasi-linear effects, full-wave code AORSA and the fi-

* One of the authors, Dan Du, would like to express gratitude to P. W. Zheng, L. Han, S. D. Song, and H. Yang for fruitful discussions. This study is supported by National magnetic confinement fusion energy development research project (2022YFE03070003 and 2022YFE03070001), the Ministry of Science and ICT under KFE R&D Programme of 'KSTAR Experimental Collaboration and Fusion Plasma Research (KFE-EN2401-15)', the National Natural Science Foundation of China (11205086 and 1227051066), Natural Science Foun- dation of Hunan Province (2020JJ4515), Key Research and development program of Anhui Province (205258180096) and Key projects of Hunan Provincial Department of Education (20A432).

† Corresponding author, sdeng@ipp.ac.cn

nite element solver COMSOL [1–4, 12, 13]. Utilizing the GENRAY/CQL3D package, simulations demonstrate an optimal launched $N_\parallel$ of approximately 1.6 for the CFETR hybrid scenario, with a maximum helicon wave current drive efficiency of $2.8 \times 10^{19}\mathrm{A}\cdot\mathrm{W}^{-1}\cdot\mathrm{m}^{-2}$ [2]. For the sample case DIII-D, the analysis reveals that the off-axis current drive is 2 to 4 times more efficient than the off-axis neutral beam current drive under the same conditions, and the helicon current drive is essentially constant for launched $N_\parallel$ between 2.8 and 4.2 [12]. Simulations on spherical tokamak NSTX upgrade show that for helicon wave heating and current drive, launching at high toroidal wave number appears to be one way to significantly reduce the ion damping and in turn to obtain large electron damping in the core [14]. To analyze the coupling between the combline antenna and VEST plasma, J. G. Jo et al used the finite element solver COMSOL to obtain the maximum helicon wave coupling with $N_\parallel \sim 4.5$ and frequency at 500 MHz [1]. Recently, C. Lau et al have performed a numerical study with the full wave code AORSA to understand the impact of SOL turbulence on helicon wave propagation and absorption in the DIII-D tokamak, and found that power loss in SOL peaked at higher fluctuation wavelength λ_{fluct} for high $N_\parallel$ [3]. The results of these studies show that helicon wave heating and current drive depend strongly on the launched $N_\parallel$ spectrum of antenna, and different fusion devices and antennas have different optimization parameters for $N_\parallel$.

EXL-50 is a new spherical tokamak designed in 2018 and built in 2019. In 2023, it was upgraded to EXL-50U with a major radius of 0.6-0.8 m, and a minor radius of 0.32-0.5 m. The primary objectives of the EXL-50U device are to achieve plasma current I_p 300-600 kA and to ensure that the ion temperature in the plasma core exceeds the electron temperature, with a target ratio of $T_i/T_e = 1.5$ [15]. Recently, it has obtained $I_p \sim 300$ kA with 1s flat-top. To achieve the experimental objectives, further research on the wave heating and current drive capability of EXL-50U is needed.

A helical TWA is mainly composed of antenna box, feed, Faraday shield, and helical line, whose structure has a certain impact on the $N_\parallel$ power spectrum, leading to the generation of some sidebands [11]. Many previous efforts have focused on studying the effects of the main peak of the antenna power spectrum on helicon wave heating and current drive. However few researches have considered the influence of the sidebands of the TWA power spectrum on helicon wave and current drive. Commercial software COMSOL can be used for handling 3D RF antenna structure with a dielectric medium or plasma loading, and obtaining the power spectrum by solving Maxwell's equation [16]. The validity and correctness of RF antenna simulations based on COMSOL have been proven by some codes [17].

Adopting the EXL-50U experimental parameters, two KSTAR-like traveling wave antennae are designed by COMSOL. By coupling the antenna power spectrum with GENRAY, the influence of sidebands of two KSTAR-like TWA on the HCD in EXL-50U plasma has been studied. The structure of this paper is as follows. In section II, we briefly describe the models and equations of helicon physics in EXL-50U plasma. A broad parametric scan of parallel refractive index, frequency, density, temperature, and magnetic field for HCD are presented in section III. In section IV, a possible physical mechanism of the influence of the sidebands on HCD is discussed. Section V presents the conclusions.

II. MODELS AND EQUATIONS

The propagation characteristics of helicon waves in plasma are sufficient to be described by a cold plasma dispersion relation, and the vertical refractive index $N_\perp$ in the plasma meets [3]:

$$
\begin{aligned}
N_{\perp\pm}^2 &= \frac{1}{2S}(S+P)(S-N_\parallel^2) - \frac{1}{2S}D^2 \\
&\pm \frac{1}{2S}\sqrt{[(S+P)(S-N_\parallel^2)-D^2]^2 + 4N_\parallel^2 D^2 P^2}
\end{aligned}
\tag{1}
$$

where the S, D and P are the elements of the cold dielectric tensor in Stix's style [18], $N_\parallel$ is the parallel refractive index. There are two different wave branches, as can be seen from Eq. (1). The first, corresponding to the minus sign is the fast wave, also known as helicon wave; the second, with the plus sign, is the slow wave. The condition for helicon wave or slow wave propagation in plasma is $N_{\perp-}^2 > 0$ or $N_{\perp+}^2 > 0$ respectively. If the frequency of helicon wave is f , the wavelength of the helicon fast wave and slow wave can be represented by $\lambda_-^{-1} = (\sqrt{N_\parallel^2 + N_{\perp-}^2}) \times f/c$, $\lambda_+^{-1} = (\sqrt{N_\parallel^2 + N_{\perp+}^2}) \times f/c$ respectively.

According to the [19], the critical parallel refractive index N_{acc} to depart the two branches can be estimated by the below formula:

$$
N_{\mathrm{acc}}^2 > \left(\frac{D^2}{\sqrt{|P|}} + \sqrt{S}\right)^2 \tag{2}
$$

which is the accessibility condition. It is well-known that the dominant damping mechanism of helicon waves is electron Landau damping and transit time magnetic damping [20]. When the phase velocity of the wave is comparable to the thermal velocity of the particle, i.e. $\omega/k_\parallel = v_{th}$, a strong Landau damping occurs between the wave and the particle. The sufficient condition for electron Landau damping absorption is $\omega/k_\parallel \leq 2.5v_{th}$ or parallel refractive index meets [21]:

$$
N_{damp} \geq \frac{2.5}{3}\frac{6.5}{\sqrt{T_e\mathrm{keV}}} \tag{3}
$$

Helicon wavelengths in EXL-50U plasma are much less than the machine size. Due to the short wavelength nature of helicon waves, the ray-tracing technique is a good approximation to calculate the HCD in EXL-50U plasma. GENRAY has several options for power absorption and current drive. The Chiu model is used for electron and ion absorption in which the code calculates the vertical component of the imaginary part of the refractive index, and the standard Ehst-Karney model is used for the current drive [22].

The density and temperature profiles can be written with

the following empirical formula [23]:

$$\begin{aligned} n_e &= (n_{ec} - n_{ea})[1-(r/a)^i]^s + n_{ea} \\ T_e &= (T_{ec} - T_{ea})[1-(r/a)^i]^s + T_{ea} \end{aligned} \tag{4}$$

In the above formula, n_{ea} and n_{ec} represent the edge and center electron density respectively, while the center and edge electron temperature are represented by T_{ec} and T_{ea} respectively, $i = 1$ and $s = 1/2$. In the following calculations, we will keep the temperature and density distribution constant, and only use the temperature and density at the center to represent the overall change.

III. NUMERICAL RESULTS

A. The influence of parallel refractive index, frequency, density, temperature on driving current of helicon waves

The double-null equilibrium configuration of the EXL-50U device was reconstructed using the EFIT program (Fig. 1(a)). The density and temperature profiles are shown in (Fig. 1(b)) and ((Fig. 1(c)). The central toroidal magnetic field, electron density, and electron temperature are 0.757 T, 6×10^{18} m^{-3}, and 1 keV, respectively. Thirty rays are set to be emitted from the low field side in the form of a Gaussian-like spectrum (Step_G for short) and the total injection power is 1 MW. The expression of the power spectrum is $P = (\sin(N_\parallel - N_{\parallel 0})/(N_\parallel - N_{\parallel 0}))^2$, $N_{\parallel 0}$ is the main peak of $N_\parallel$.

Fig. 2 presents the relationships between driving current, parallel refractive indices $N_\parallel$ and frequency with $n_{ec} = 6 \times 10^{18}$ m^{-3} , $T_{ec} = 1\mathrm{keV}$. Because the equilibrium magnetic field is in a counterclockwise direction, negative values are assigned to $N_\parallel$ in the simulations to yield a positive driven current. It can be seen that when the frequency is 300 MHz-500 MHz, the helicon driven current first increases and then decreases, which peaks around $N_\parallel$ = 3-3.4 at 400 MHz-500 MHz. Therefore, for the engineering design of the helicon system on EXL-50U, the value of $N_\parallel$ should be set around -3.2 to obtain a higher drive current when the frequency is above 400 MHz.

Fig. 3 shows the helicon wave propagation domain and wavelengths in the EXL-50U plasma density-magnetic field strength plane with f = 476 MHz. The area surrounded by two thick black lines is transparent for the helicon wave where $N_{\perp -}^2 > 0$, the threshold densities for excitation of the helicon wave are gradually increased with magnetic fields (Fig. 3(a)). The wavelength decreases with increasing density and increases with increasing magnetic field (Fig. 3(b)). When the magnetic field varies between 0.3-0.757 T, the densities for propagation of the helicon wave are $4.2 \times 10^{18}\mathrm{m}^{-3} - 2.69 \times 10^{19}\mathrm{m}^{-3}$, and the wavelengths are less than 0.08 m.

Fig. 4 illustrates the relationships between the driven current, electron density and temperature with f= 476 MHz, $N_\parallel = -3.2$. Simulation results demonstrate that the driven current has a relatively stable upward trend with increased plasma temperature, but shows an overall decrease with increasing density. It is worth noting that the helicon wave can drive a substantial current at lower densities. For instance, at density of 5.4×10^{18} m^{-3}, 1 MW helicon wave can drive approximately 500 kA current with $T_{ec} = 1.1$ keV, and the corresponding dimensionless efficiency is $\zeta \equiv \frac{e^3}{\epsilon_0^2}\frac{nIR}{PKT} \equiv 33\frac{n_{20}I_A R_m}{P_W T_{KeV}} = 0.53$ which remains notably significant compared to the high current drive efficiency $\zeta = 0.64$ observed in the previous DIII-D tokamak experiments.

B. The effect of spectrum sidebands on the helicon wave current drive

Based on the simulation results presented above, it is evident that when the frequency and $|N_\parallel|$ range from 400 MHz to 500 MHz, 3 to 3.4, respectively, a relatively higher helicon wave drive current is achieved. Next, two sets of KSTAR-like [11] helical traveling wave antennas are designed using COMSOL, labeled as A and B, with a spectral peak of $N_\parallel = -3.2$ and a frequency of 476 MHz (Fig. 5 and Fig. 6). Antennas A and B have ten and six current bands respectively. The spacing between adjacent current bands is equal and labeled as D, for a single turn of the helical line, the dimensions of L_1, L_2, and D for A and B are 270 mm, 146 mm, 52 mm and 270 mm, 140 mm, 52 mm, respectively.

Fig. 6 shows the radiation power spectra of the KSTAR-like helical traveling wave antennas A (Step_A) and B (Step_B), along with a Gaussian-like spectrum (Step_G). The parallel refractive indices corresponding to the main peaks (position 1) of these three spectra are all $N_{\parallel\_1} = -3.2$, the primary difference among these three spectra is the intensity and quantity of sidebands. Both Step_A and Step_B spectra have secondary peaks (position 2) with relatively high energy, whose parallel refractive indices are $N_{\parallel\_2} = 8.6$. The term 'spectral width' refers to the width between two points where the power spectrum intensity is at half of its maximum. The spectral width of the main peak follows the order: Step_A < Step_B < Step_G , and the spectral width of the secondary peak in Step_A is smaller than that in Step_B.

To study the influence of sidebands on HCD, the antenna spectrum and GENRAY program are coupled. In Fig. 7, a total of 30 rays were emitted from the low-field side with injection power of 1 MW, the energy spectrum of 30 rays is a fitting function of the antenna radiation spectrum at t = 0. Fig. 8 and Fig. 9 depict the relationships between the driven currents of Step_A, Step_B, and Step_G, density and temperature. ΔI_{AG} and ΔI_{BG} respectively represent the driven current differences between Step_A and Step_G and between Step_B and Step_G, with their maximum values denoted as ΔI_{max_AG} and ΔI_{max_BG}. The simulations indicate that when the magnetic field (the center magnetic field is B_0) remains constant, within a specified range of temperature (0.6 keV-1.4 keV) and density 4.2×10^{18} $\mathrm{m}^{-3} - 1.2 \times 10^{19}$ m^{-3}, as the temperature rises, the impact of the sidebands on the HCD intensifies (Fig. 8 and Fig. 9). In some density cases, the impact of the sideband on HCD can not be ignored. For example, at the present classical order of density, when the $n_{ec} = 7.8 \times 10^{18}$ m^{-3}, the influence of the sidebands on the HCD increases significantly. Maximum differences

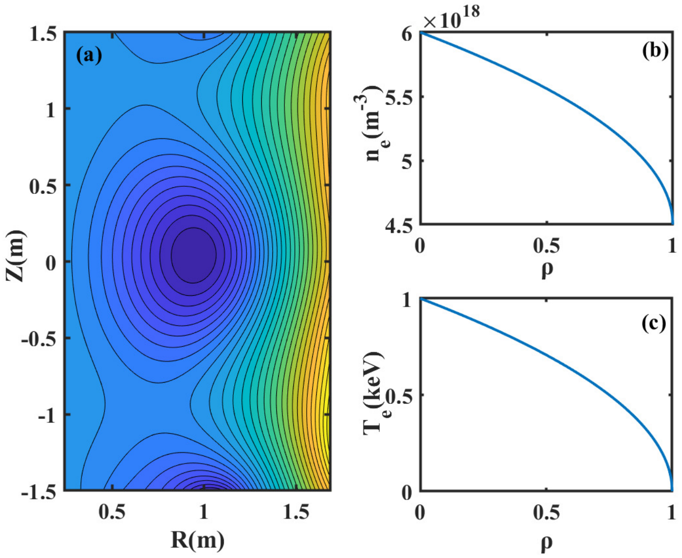

Fig. 1. (a) Configuration, profiles of (b) density and (c) temperature of the EXL-50U.

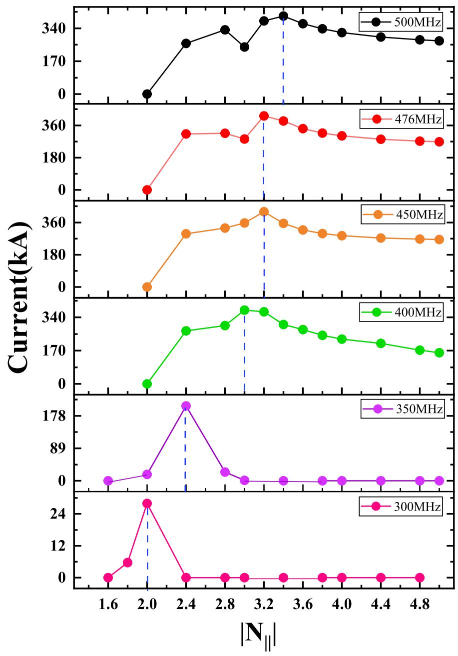

Fig. 2. Dependence of driven current on $N_{||}$ at different frequencies.

ΔI_{max_AG} and ΔI_{max_BG} reach 91.281 kA and 87.137 kA, respectively, while minimum values are -49.355 kA and -44.034 kA as shown in Fig. 9. Also, when increasing the operating density of the device, special attention should be paid to the impact of the sideband on HCD. As shown in the Fig. 9, when the the $n_{ec} = 1.2 \times 10^{19}\ \mathrm{m}^{-3}$, the impact of the sideband on HCD is particularly larger, maximum differences ΔI_{max_AG} and ΔI_{max_BG} reach 67.232 kA and 73.308 kA, respectively. In the green and dark green areas of Fig. 9, the driven currents of $\mathrm{Step\_A}$ and $\mathrm{Step\_B}$ are greater than the Gaussian-like spectrum $\mathrm{Step\_G}$, and the driven current of $\mathrm{Step\_A}$ is slightly larger than that of $\mathrm{Step\_B}$. This implies that to achieve a relatively high driven current, the spectral width should not be too wide.

Fig. 10 presents the influence of magnetic field on HCD under four density temperature conditions. Simulation results indicate that in low-density plasma ($n_{ec} = 4.2 \times 10^{18}\ \mathrm{m}^{-3}$), when the central magnetic field is below 1.3 T, the influence of the sidebands on the helicon wave current drive is minimal. However, when the central magnetic field exceeds 1.3 T, the impact of the sidebands on the current drive increases(shown in Fig. 10 (a) and (b)). The changing trend is

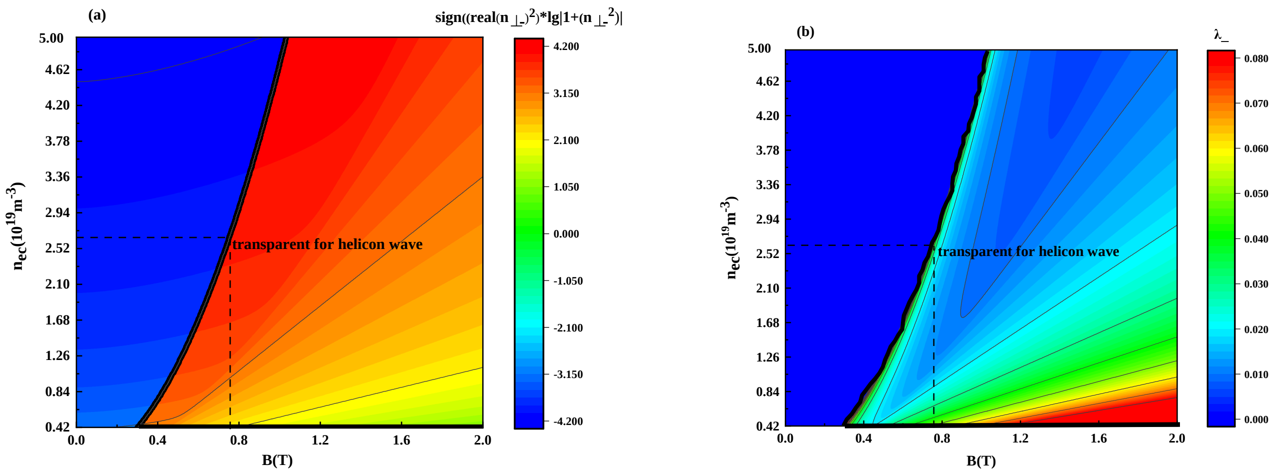

Fig. 3. Helicon wave propagation domain and wavelengths in the EXL-50U plasma density-magnetic field strength plane.

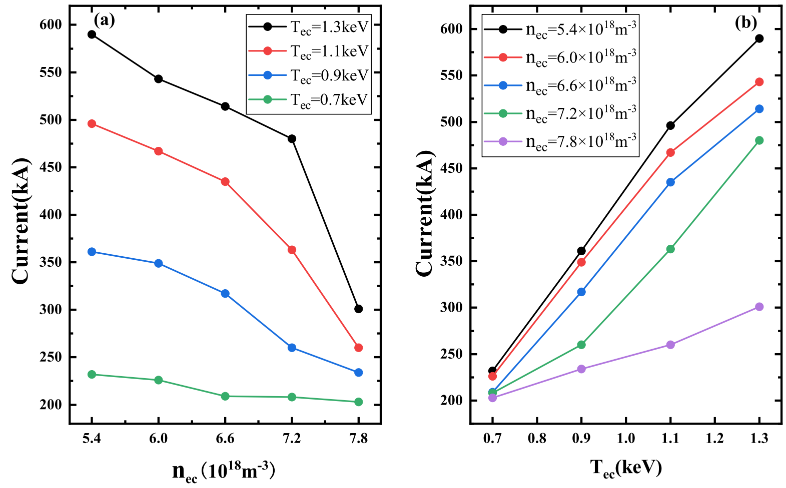

Fig. 4. Helicon wave (476 MHz) driven current as functions of core temperature and density plasma.

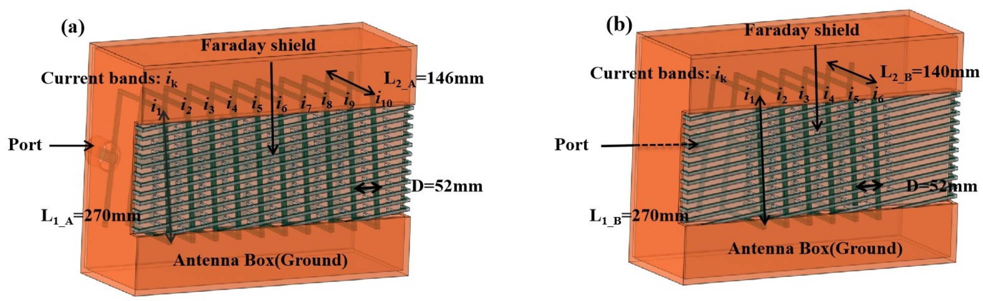

Fig. 5. Basic structure of KSTAR-like TWA (a) A, (b) B.

opposite in medium-density plasma ($n_{ec} = 7.8 \times 10^{18}\ \mathrm{m}^{-3}$), the influence of the sidebands on HCD is small when the central magnetic field is above 1.3 T, and increases when it is below 1.3 T (shown in Fig. 10 (c) and (d)). The increase in temperature increases the impact of sidebands on HCD to some extent. As the temperature rises, the impact of the sidebands on the HCD intensifies. For example, when the $n_{ec} = 4.2 \times 10^{18}\ \mathrm{m}^{-3}$, as the temperature rises from 0.7 keV to 1.2 keV, the difference in driving current for Step_A, Step_B, and Step_G is pronounced, with $|\Delta I_{max\_AG}|$ and $|\Delta I_{max\_BG}|$ increasing from 61 kA and 57 kA to 72 kA and 75 kA, respectively (as shown in Fig. 10 (a) and (b));

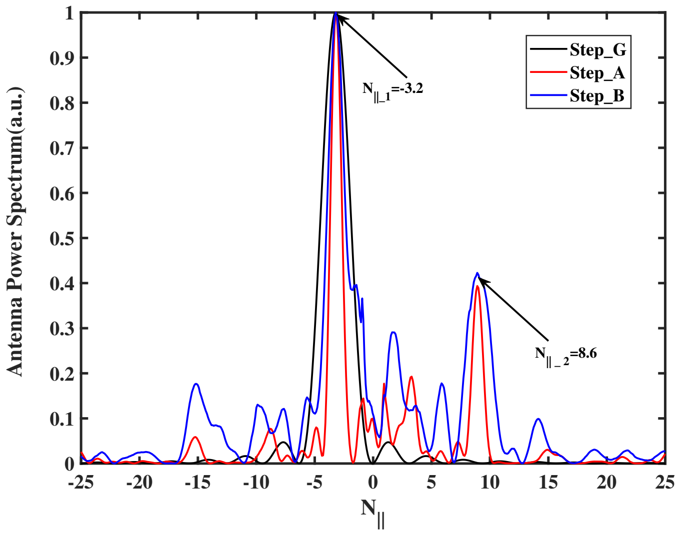

Fig. 6. $N_{\|}$ power spectra for Step_A, Step_B and Step_G.

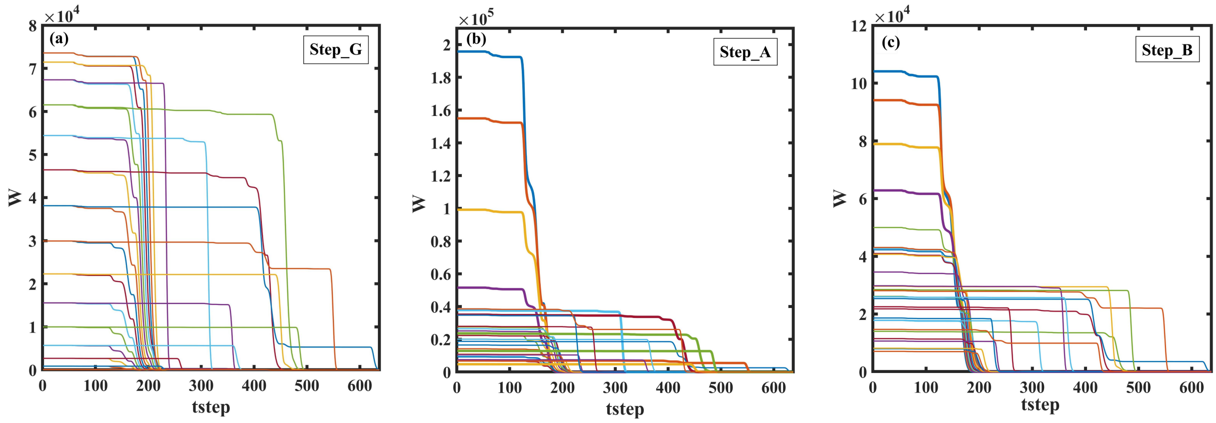

Fig. 7. The variation of power in each ray over time with $n_{ec} = 7.8 \times 10^{19}\ \mathrm{m}^{-3}$, $T_{ec} = 1.1\ \mathrm{keV}$, $B = 1\mathrm{B}_0$, $N_{\|} = -3.2$. (a) Step_G, (b) Step_A and (c) Step_B.

when the $n_{ec} = 7.8 \times 10^{18}\ \mathrm{m}^{-3}$ the difference in driving current for Step_A, Step_B, and Step_G is more pronounced, with ΔI_{max_AG} and ΔI_{max_BG} increasing from 112 kA and 104 kA to 178 kA and 166 kA, respectively (as shown in Fig. 10(c) and (d)).

Fig. 11 shows that when the the $T_{ec} = 1.4\ \mathrm{keV}$ remains constant, the relationships between the driven current differences ΔI_{AG} and ΔI_{BG}, density and magnetic field. In medium-density low-magnetic-field plasma and relatively low-density high-magnetic-field plasma, the influence of the sidebands on HCD intensifies. The largest difference ΔI_{max_AG} and ΔI_{max_BG} respectively reach 177.820 kA and 165.178 kA in the deep green region of Fig. 11, and -165.741 kA and -123.675 kA in the yellow portion.

Fig. 12 shows the drive current profiles of Step_A, Step_B, and Step_G. Case 1, the parameters are $n_{ec} = 4.2 \times 10^{18}\ \mathrm{m}^{-3}$, $T_{ec} = 0.7\ \mathrm{keV}$, $B = 2.25 B_0$. Case 2, the parameters are $n_{ec} = 7.8 \times 10^{18}\ \mathrm{m}^{-3}$, $T_{ec} = 0.9\ \mathrm{keV}$, $B = 1 B_0$. The simulation results indicate that, under specific conditions, the sidebands of Step_A and Step_B influence not only the magnitude of HCD, but also the profile of the driven current, causing the peak of the current profile to shift toward the center or the edge (see Fig. 12). For example, if the antenna spectrum changes from Step_G to Step_A, the current peak shifts from the normalized radius of 0.32 to 0.13 for case 1 (Fig. 12(a)), and 0.1075 to 0.1225 for case 2 (Fig. 12(b)). The current peak's positions of Step_A and Step_B are close to each other, but Step_B's current distribution disperses towards the edge, resulting in a lower driven current peak compared to Step_A, indicating poor locality (Fig. 12(a)). This indicates that under certain conditions, antenna spectrum with narrow sidebands can not only enhance the drive current to a certain extent but also increase the locality of the current distribution, which is beneficial for local control.

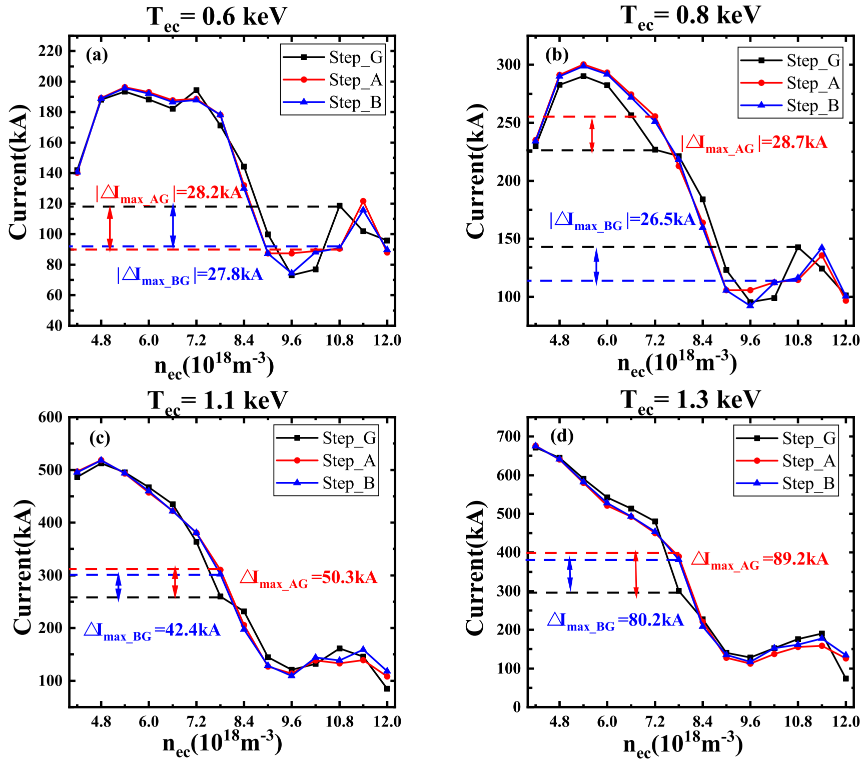

Fig. 8. Dependence of the driven current with density for different $N_{\parallel}$ power spectra. (a) T_{ec} = 0.6 keV, (b) T_{ec} = 0.8 keV, (c) T_{ec} = 1.1 keV, (d) T_{ec} = 1.3 keV.

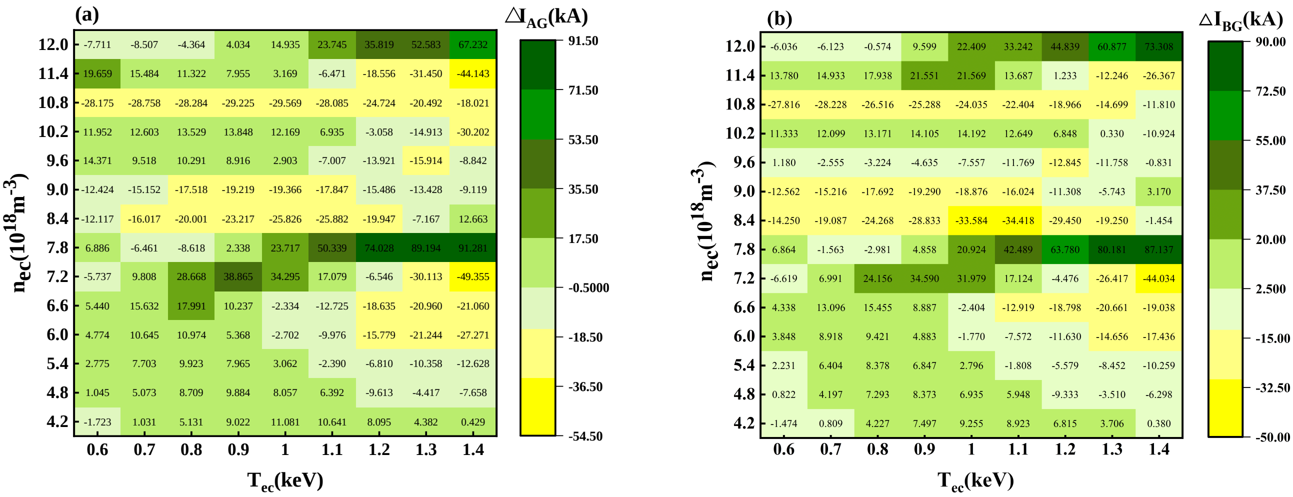

Fig. 9. The relationships between the driven current differences ΔI_{AG} and ΔI_{BG}, density and temperature.

IV. DISCUSS

To reveal the physical mechanism of the influence of sidebands on HCD, this paper next simulated two rays' current profiles, the wave trajectories in the polar cross-section, and the variations of the Landau refractive index N_{damp}, accessibility condition N_{acc} , parallel refractive index $N_{\parallel}$ along with the propagation distance for case 1 and case 2 (Fig. 13-Fig. 15). These two rays correspond to the main peak and secondary peak of Step_A and Step_B, with $N_{\parallel\_1} = -3.2$ and $N_{\parallel\_2} = 8.6$, respectively. The simulations show that when the two rays propagate in the plasma, their lower limits meet accessibility condition, and $N_{\parallel}$ gradually shifts up as the propagation distance increases. The parallel refractive index $N_{\parallel\_2}$ is close to N_{damp}, which enables the ray to meet the strong Landau damping condition over a short propagation distance, and

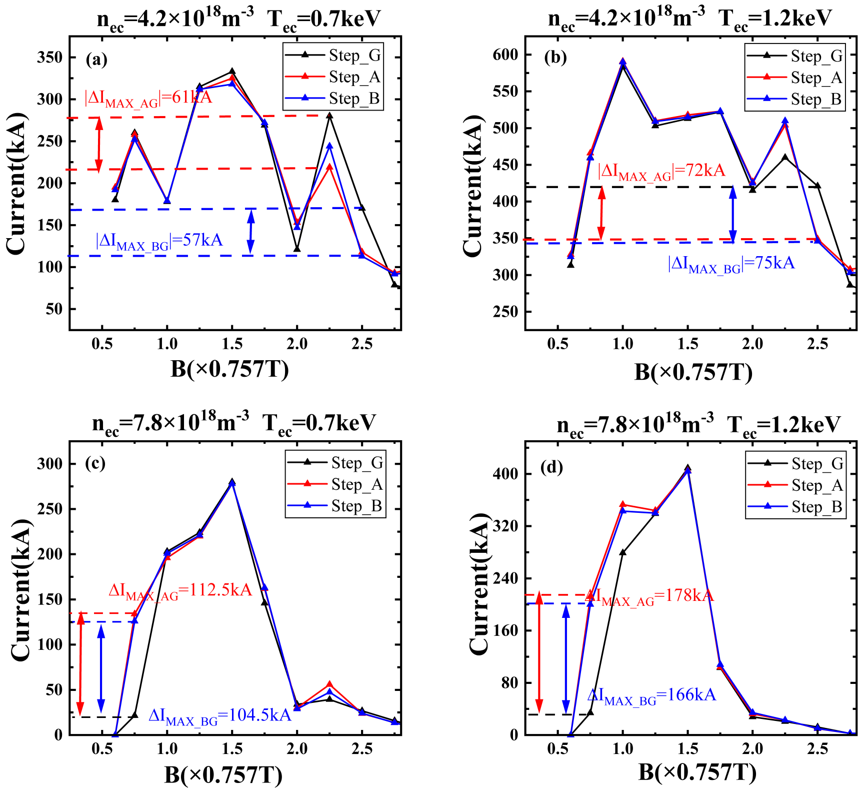

Fig. 10. Dependence of the driven current with magnetic field for three $N_{\|}$power spectra. (a) $n_{ec} = 4.2 \times 10^{18}\ \mathrm{m}^{-3}$, $T_{ec} = 0.7$ keV, (b) $n_{ec} = 4.2 \times 10^{18}\ \mathrm{m}^{-3}$, $T_{ec} = 1.2$ keV, (c) $n_{ec} = 7.8 \times 10^{18}\ \mathrm{m}^{-3}$, $T_{ec} = 0.7$ keV, (d) $n_{ec} = 7.8 \times 10^{18}\ \mathrm{m}^{-3}$, $T_{ec} = 1.2$ keV.

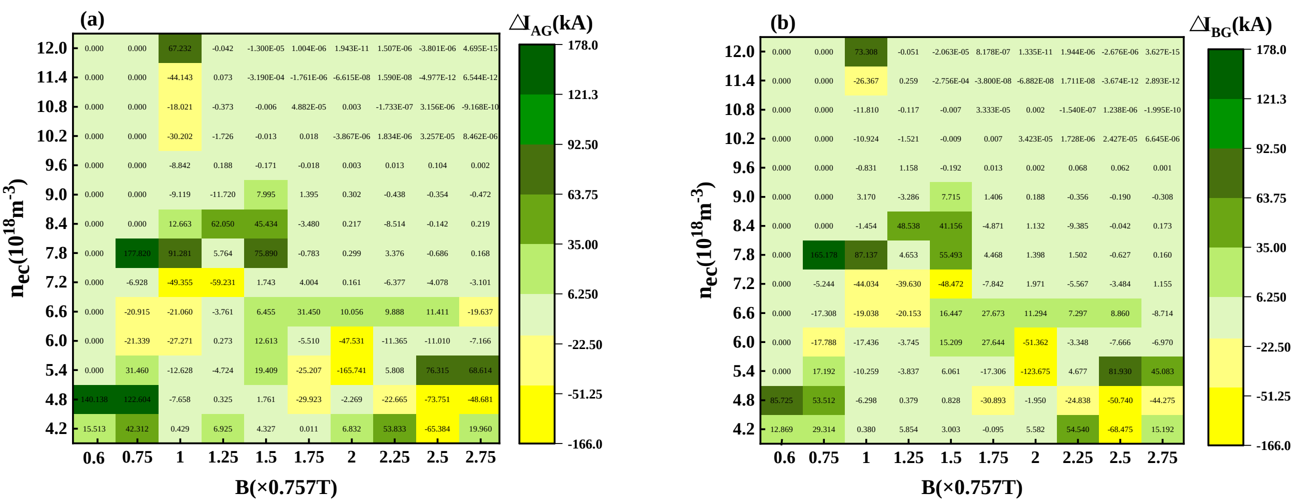

Fig. 11. Difference between the driven current of the three power spectra at different density and magnetic field.

quickly deposit near the core (Fig. 14(b) and (d) , Fig. 15(b) and (d)). Due to a significant difference between $N_{\|_{\text{-}1}}$ and N_{damp} , the ray travels a relatively long distance before depositing into the plasma. When the plasma parameters change from case 1 to case 2, the drive current peak of the ray with $N_{\|_{\text{-}1}} = -3.2$ changes from 255 A cm^{-2} to 555 A cm^{-2}, and its position moves from normalized small radius 0.31 to 0.07 (Fig. 13). The driven current profile of $N_{\|_{\text{-}2}} = 8.6$ ray is less sensitive to plasma parameters than that of $N_{\|_{\text{-}1}} = -3.2$ ray, showing a single peak in the current with minor radial distribution range changes (at normalized small radius 0.24-0.27), effectively maintaining locality. And the driven current magnitude of $N_{\|_{\text{-}2}} = 8.6$ ray is smaller than that of$N_{\|_{\text{-}1}} = -3.2$ ray (Fig. 13).

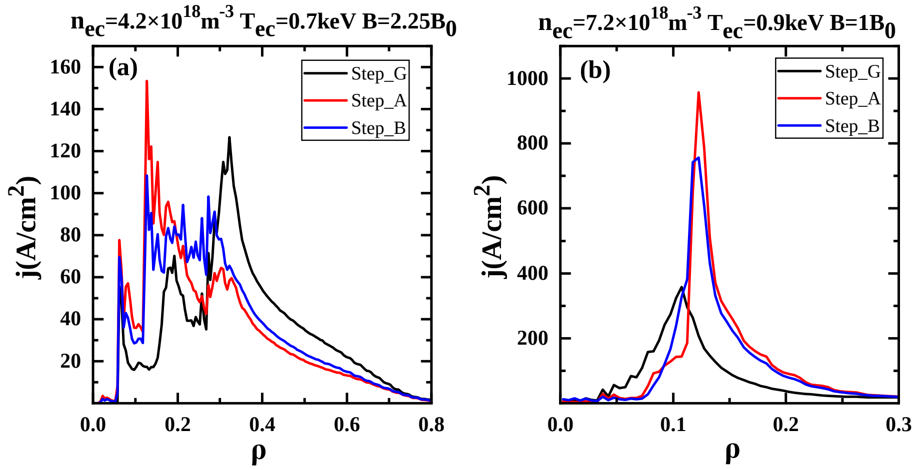

Fig. 12. Current profiles of three $N_{\|}$ power spectra. (a) $n_{ec} = 4.2 \times 10^{18}$ m^{-3}, $T_{ec} = 0.7$ keV, $B = 2.25B_0$. (b) $n_{ec} = 7.2 \times 10^{18}$ m^{-3}, $T_{ec} = 0.9$ keV, $B = 1B_0$.

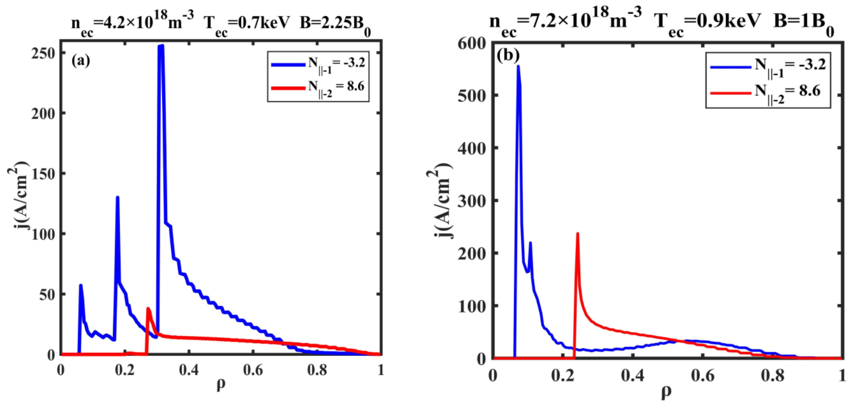

Fig. 13. Current profiles of $N_{\|}$ equal to -3.2 and 8.6. (a) Case 1, (b) case 2.

From the dispersion relation Eq. (1) and Fig. 14 and Fig. 15, it is known that plasma parameters such as magnetic field and density affect $N_{\|}$ upward or downward shift in plasma. The shorter the propagation distance of the ray, the smaller the influence of the plasma parameters on $N_{\|}$ upward or downward shift. Ray with $N_{\|_{\text{-}1}} = -3.2$, being far from strong damping condition, propagates over a considerable distance before being absorbed by the plasma. Consequently, the parallel refractive index undergoes multiple shifts, rendering the effect of the driven current on plasma parameters more sensitive. On the contrary, the strongly damped ray with $N_{\|_{\text{-}2}} = 8.6$ is absorbed over a short propagation distance, so the upward or downward shift of the parallel refractive index is less affected by plasma parameters, leading to the generation of stable and strong localized driven current profile.

From the above analysis, it can be seen that one of the important factors affecting HCD under different parameters is the main peak of the antenna spectrum. Due to the stability and locality of the driven current by the rays satisfying strong damping condition, the presence of certain sidebands being close to strong damping condition in the antenna spectrum may be beneficial for HCD, which may improve the driving current magnitude and enhance current locality control under certain conditions.

V. SUMMARY

This study investigates the influence of two KSTAR-like helical TWAs spectra sidebands on HCD in spherical torus plasma EXL-50U. Firstly, under certain conditions, the effects of parallel refractive index, frequency, temperature, and density on HCD are analyzed. It is found that when the frequency, $|N_{\|}|$, temperature and density satisfy 300 MHz $\leq f \leq$ 500 MHz, $3 \leq |N_{\|}| \leq 3.4$, 0.7 keV $\leq T_{ec} \leq$ 1.3 keV, 5.4×10^{18} $\mathrm{m}^{-3} \leq n_{ec} \leq 7.8 \times 10^{18}$ m^{-3}, respectively, helicon wave can obtain relatively high driven current in EXL-50U plasma, around 200 kA-600 kA.

Then, on this basis, two sets of 476 MHz KSTAR-like TWAs are designed for EXL-50U by COMSOL, whose spec-

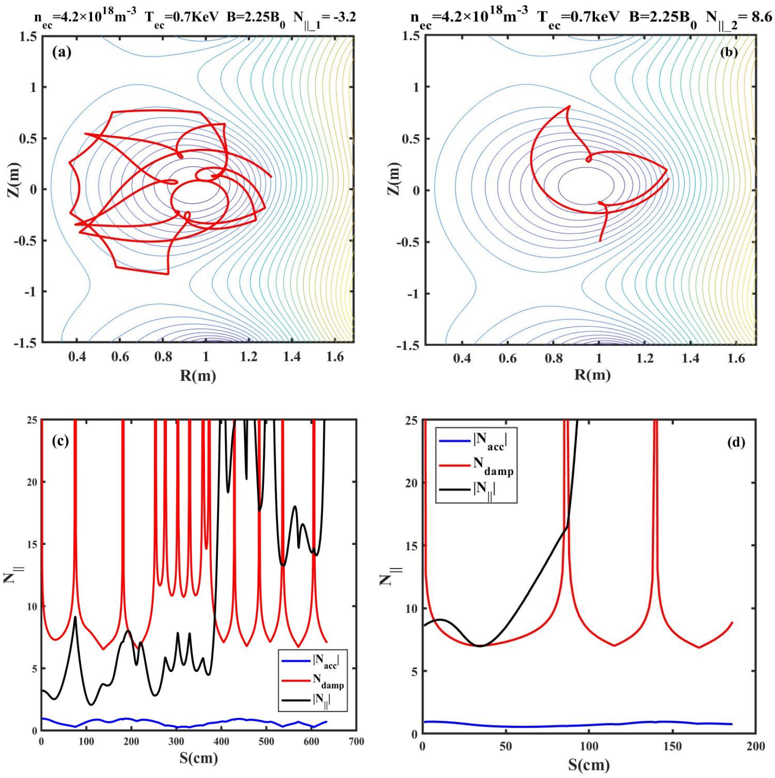

Fig. 14. Ray trajectories in polar cross-section and the relationships between N_{damp} , N_{acc} , $N_{\|}$ and propagation distant of two rays for case 1. (a) , (c) $N_{\|\_1} = -3.2$; (b) , (d) $N_{\|\_2} = 8.6$.

tra have the same $N_{\|} = -3.2$ corresponding to the main peak and different sidebands. By coupling their spectra with GENRAY, and comparing HCD driven by them with by Gaussian-like spectrum, the influence of sidebands of two KSTAR-like TWAs on HCD in EXL-50U plasma has been studied. When the central temperature, density, and magnetic field strength vary within the range of $0.6\ \mathrm{keV} \leq T_{ec} \leq 1.4\ \mathrm{keV}$, $4.2 \times 10^{18}\ \mathrm{m}^{-3} \leq n_{ec} \leq 1.2 \times 10^{19}\ \mathrm{m}^{-3}$, $0.4542\ \mathrm{T} \leq B \leq 2.082\ \mathrm{T}$, respectively, the simulation results indicate:

1) Under medium-density low-magnetic-field and low-density high-magnetic-field conditions, the influence of the sidebands on HCD is significant, with the largest difference of 178 kA for these three spectra' driven currents under the same injection power.

2) Under certain conditions, the higher the temperature, the greater the impact of the spectral sidebands on HCD.

3) The sidebands not only affect the magnitude of the HCD, but also cause the current peak to shift towards the center or edge (Fig. 12). Narrow sidebands with parallel refractive index close to the strong Landau damping condition may improve the driven current magnitude and localized control, which may be beneficial for HCD.

Finally, the physical mechanism of the influence of the sidebands on HCD is discussed: plasma parameters such as magnetic field and density affect $N_{\|}$ upward or downward shift in plasma.The shorter the propagation distance of the ray, the smaller the influence of the plasma parameters on $N_{\|}$ upward or downward shift. Rays being close to strong damping condition, are absorbed over a short distance, resulting in their parallel refractive index being less affected by plasma parameters and achieving stable and strong localized HCD. Consequently, under certain conditions, if the antenna spectrum has narrow sidebands with parallel refractive index close to the strong Landau damping condition, it is maybe beneficial for improving driven current magnitude and local control. Related research provides certain guidance for the design of RF antenna and HCD experiments.

[1] J.G. Jo, J. Wang, H.W. Lee et al., Coupling study of fast wave near the lower hybrid frequency range in VEST. Phys. Plasmas **25**, 082511 (2018). doi: 10.1063/1.5037370

[2] X.S. Wu, J.C. Li, J.L. Chen et al., Parametric study of helicon wave current drive in CFETR. Nucl. Fusion **63**, 106015 (2023). doi: 10.1088/1741-4326/ACF231

[3] C. Lau, M. Brookman, A. Dimits et al., Helicon full-wave modeling with scrape-off-layer turbulence on the DIII-D tokamak. Nucl. Fusion **61**, 126072 (2021). doi: 10.1088/1741-4326/AC36F3

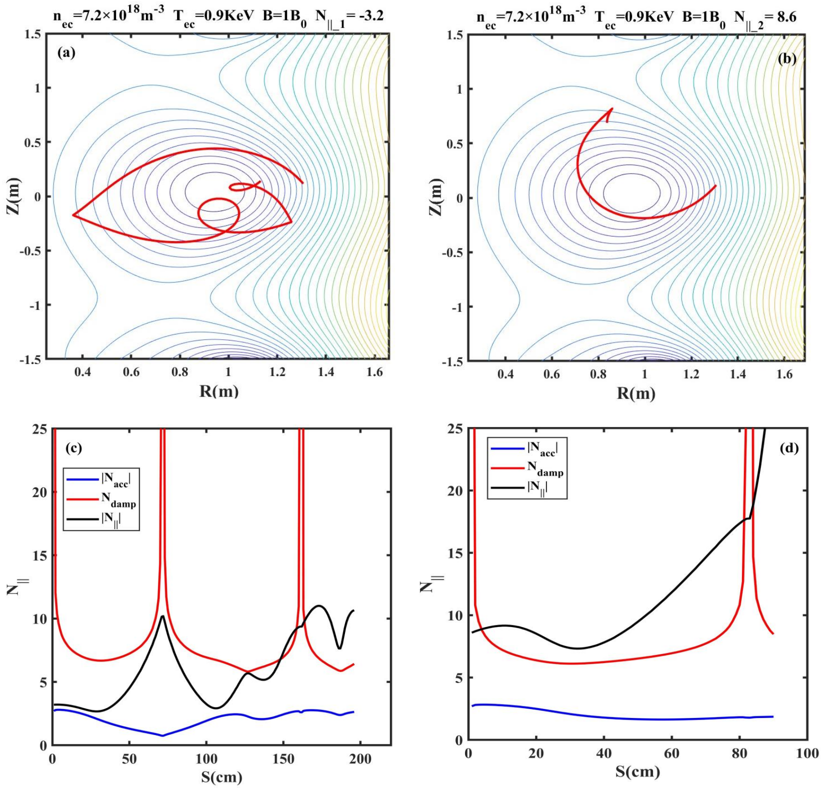

Fig. 15. Ray trajectories in polar cross-section and the relationships between N_{damp} , N_{acc} , $N_{\|}$ and propagation distant of two rays for case 2. (a) , (c) $N_{\|\_1} = -3.2$; (b) , (d) $N_{\|\_2} = 8.6$.

[4] S.J. Wang, J. Kim, J.H. Jeong et al., Recent experimental results of KSTAR RF heating and current drive. AIP Conf. Proc. **1689**, 030014 (2015). doi: 10.1063/1.4936479

[5] J.R. Wilson, R.E. Bell, S. Bernabei et al., Exploration of high harmonic fast wave heating on the National Spherical Torus Experiment. Phys. Plasmas **10**, 1733 (2003). doi: 10.1063/1.1560921

[6] S.C. Jardin, C.E. Kessel, C.G. Bathke et al., Physics basis for a reversed shear tokamak power plant. Fusion Eng. Des. **38**, 27 (1997). doi: 10.1016/S0920-3796(97)00111-7

[7] T. Ogawa, K. Hoshino, S. Kanazawa et al., Radiofrequency experiments in JFT-2M: Demonstration of innovative applications of a travelling wave antenna. Nucl. Fusion **41**, 1767 (2001). doi: 10.1088/0029-5515/41/12/304

[8] C.B. Van, M.W. Brookman, C.P. Moeller et al., The high-power helicon program at DIII-D: gearing up for first experiments. Nucl. Fusion **61**, 116034 (2021). doi: 10.1088/1741-4326/AC25C0

[9] H.Y. Lee, J.H. Kim, H.H. Wi, et al., RF conditioning to suppress multipactor discharge for helicon wave current drive in KSTAR. Fusion Eng. Des. **193**, 113782 (2023). doi: 10.1016/J.FUSENGDES.2023.113782

[10] A. Nagy, J. deGrassie, C. Moeller et al., A high power helicon antenna design for DIII-D. Fusion Sci. Technol. **72**, 623 (2017). doi: 10.1080/15361055.2017.1347459

[11] H.H. Wi, S.J. Wang, J. Kim et al., RF design of helical long-wire traveling wave antenna for helicon current drive in KSTAR. Fusion Eng. Des. **195**, 113983 (2023). doi: 10.1016/J.FUSENGDES.2023.113983

[12] R. Prater, C.P. Moeller, R.I. Pinsker et al., Application of very high harmonic fast waves for off-axis current drive in the DIII-D and FNSF-AT tokamaks. Nucl. Fusion **54**, 083024 (2014). doi: 10.1088/0029-5515/54/8/083024

[13] G.J. Qiao, D. Luo, S.D. Song et al., Performance assessment of helicon wave heating and current drive in EXL-50 spherical torus plasmas. J.Fusion Energy **42**, 28 (2023). doi: 10.1007/S10894-023-00366-8

[14] N. Bertelli, M. Ono E.F. Jaeger, Modeling of high harmonic fast wave scenarios for NSTX Upgrade. Nucl. Fusion **59**, 086006 (2019). doi: 10.1088/1741-4326/ab1d7f

[15] H.J. Ma, H.S. Xie, B. LI, Simulation of ion cyclotron wave heating in the EXL-50U spherical tokamak based on dispersion relations. Plasma Sci. Technol. **26**, 025105 (2024). doi: 10.1088/2058-6272/AD0D53

[16] H. Zhou, D. Du, Z.S. Yang et al., 3D electromagnetic simulation of the coupling characteristics and double-stub FT impedance matching for EAST ICRH four-strap antenna. Plasma Sci. Technol. **26**, 005000(2024). doi: 10.1088/2058-6272/ad68ad

[17] D. Du, K. Saito, J.G. Kwak et al., Design of an optimized load-resilient conjugate T for the ICRH system in the LHD using a novel hybrid circuit/3DLHDAP code and experimental results. Nucl. Fusion **63**, 126027 (2023). doi: 10.1088/1741-4326/ACF5FE

[18] T.H. Stix, Waves in Plasmas (Springer Verlag, New York, 1992). (in English)

[19] R.I. Pinsker, Whistlers, helicons, and lower hybrid waves: the physics of radio frequency wave propagation and absorption for current drive via Landau damping. Phys. Plasmas **22**, 090901 (2015). DOI: 10.1063/1.4930135

[20] M. Ono, High harmonic fast waves in high beta plasmas. Phys. Plasmas **2**, 4075 (1995). doi: 10.1103/PhysRevC.74.054612
[21] M.H. Li, Dissertation, University of Chinese Academy of Sciences, 2012
[22] S.C. Chiu, V.S. Chan, R.W. Harvey et al., Theory of fast wave current drive for tokamak plasmas. Nucl. Fusion **29**, 2175 (1989). doi: 10.1103/PhysRevC.88.044612
[23] J.C. Li, X.T. Ding, J.Q. Dong et al., Helicon wave heating and current drive in toroidal plasmas. Plasma Phys. Control. Fusion **62**, 095013 (2020). doi: 10.1088/1361-6587/aba367